MULTIRESOLUTION ANALYSIS OF ELASTIC DEGRADATION IN HETEROGENEOUS MATERIALS [1]

Kaspar Willam, Inkyu Rhee and Gregory Beylkin

University of Colorado at Boulder, Boulder CO 80309-0428, USA

Abstract :

In this study we examine the stiffness properties of heterogeneous elastic materials and their degradation at different levels of observations. To this end we explore the opportunities and limitations of multiresolution wavelet analysis, where successive Haar transformations lead to a recursive separation of the stiffness properties and the response into coarse- and fine-scale features. In the limit, this recursive process results in a homogenization parameter which is an average measure of stiffness and strain energy capacity at the coarse scale.

The basic concept of multiresolution analysis is illustrated with one- and two-dimensional model problems of a two-phase particulate composite representative of the morphology of concrete materials. The computational studies include the microstructural features of concrete in the form of a bi-material system of aggregate particles which are immersed in a hardened cement paste taking due account of the mismatch of the two elastic constituents.

Keywords :

Multiresolution Homogenization, Haar Wavelets, Damage Mechanics of Coarse and Fine Scale Features.

1.0 Introduction

Traditionally, engineering materials are considered to be macroscopically homogeneous and often isotropic. While in most applications this approach may be adequate, progressive degradation processes can only be explained properly by considering micro-structural events which take place at the fine scales of materials. This requires characterization of each constituent and their interface conditions, in addition to the morphology of the specific meso- and micro-structures, respectively. This type of study is very demanding

---

in terms of manpower and computing resources, in spite of the recent computational advances in model-based simulations in three-dimensional space and time.

Modern deterioration analysis involves many disciplines, whereby two interactions are of particular importance:

(a) Multi-Physics Interaction

Deterioration of materials is induced by the mismatch of the constituents in heterogeneous materials and environmental factors, which include temperature, humidity, and various types of aggressive chemicals governed by coupled diffusion processes (heat conduction, moisture diffusion and mass transfer). Mechanical damage in the form of distributed micro defects interacts with the environmental factors which accelerate mechanical deterioration and vice versa. These multiple interaction phenomena have opened up and created an entirely new field of research because coupled hygro-thermo-chemo-mechanical damage processes are significantly different from traditional structural and material mechanics problems that have been dealt with so far.

(b) Multiscale Interaction

The mechanical response behavior of materials arises from multiple length scales, with damage initiating at the fine scale of micro-defects. In contrast, the response of materials due to diffusion controlled processes can be traced down to nanometer level. This is because the morphology of the complex network of very fine pores in concrete materials has a dominant effect on mass transfer and ion permeation. The correlation between the multiple scales is a new research topic for materials research community. The actual implementation of multiscale deterioration mechanisms in computational platforms is a big challenge to the community concerned with deterioration processes.

From a practical point of view, the engineering community needs macroscopic descriptions of damage at the continuum level at which the effect of microdefects are homogenized. In the parlance of structural engineering we need a coarse representation of degradation when we want to predict the life-cycle performance of large scale infrastructures such as bridges, dams etc. Therefore, the question arises how to represent the degradation effects which initiate at a much finer scale and which might evolve into a macroscopic defect at the continuum level. This question has been addressed extensively by the composite mechanics community which has focused on the development of effective stiffness properties which are equivalent to the heterogeneous properties of the constituents. Different concepts of homogenization have been proposed in the past, which work well as long as we consider representative volume elements, RVE's, which are sufficiently large to ascertain statistical uniformity of distributed microdefects. These homogenization techniques reach their limitations, when we establish strength and ductility limiters of the coarse-scale material properties which are normally governed by failure processes of fine-scale material features introducing localization and loss of statistical homogeneity. In other terms, the progression of damage introduces non-positive stiffness

properties when failure scenarios are considered at the microscopic constituent level which delimit the strength and more importantly the ductility, i.e. the deformation capacity of the macroscopic continuum. It is this degradation scenario, which normally starts in the weak interface layer between the material constituents, which is of critical importance for the performance at the macroscopic continuum level. Therefore, the main issue is, whether loss of ellipticity, loss of convexity, or equivalent loss of positive definiteness of the tangential stiffness properties at the fine scale leads to the formation of strong discontinuities at the coarse scale, see Rizzi, Maier and Willam [1996]. Thereby the central objective is to isolate the positive from the non-positive properties. This is exactly the spirit of multiresolution wavelet analysis to separate the coarse low frequency response from the fine high frequency features associated with loss of ellipticity.

2. Partitioning

Aside from the challenge of modeling progressive damage, there are several significant mathematical issues which are central to the entire field of deterioration analysis. One of them deals with upscaling the fine resolution of heterogeneities to the coarse system of homogenized materials. The other deals with the loss of positive material properties when damage and degradation takes place at the fine level of observation and its manifestation at the coarse level of homogenization.

2.1 Two-Scale Scale Analysis

The mathematical background of deterioration analysis centers around two concepts, (i) partitioning of the algebraic/differential system which turns increasingly ill-conditioned as the elastic stiffness properties deteriorate, and (ii) measuring deterioration in space and time in terms of effective damage measures at different scales.

   Partitioning dates back to early work of Schur [1917] who among many important contributions to matrix analysis decomposed the solution domain into non-overlapping subdomains. In the elementary example of a linear algebraic problem the unknown solution vector r is decomposed into two groups of unknowns r_1, r_2, which describe the coarse and fine scale response in the case of wavelet transformations discussed later on.

$$\begin{bmatrix} K_{11} & K_{12} \\ K_{21} & K_{22} \end{bmatrix} \begin{bmatrix} r_1 \\ r_2 \end{bmatrix} = \begin{bmatrix} f_1 \\ f_2 \end{bmatrix} \tag{1}$$

In the case of environmental and mechanical deterioration, the solution domain decomposes naturally into:

  (a) *Multi-Physics Partitions:* interaction among mechanical damage and and environmental diffusion. In this case r_1 denote the mechanical and r_2 the environmental

unknowns, while $\boldsymbol{K}_{12}, \boldsymbol{K}_{21}$ describe the coupling between mechanical and environmental processes. The latter is normally governed by diffusion processes which take place at much finer scales than mechanical degradation.

(b) *Multi-Constituent Partitions:* interaction among the constituents of multi-phase materials, e.g. when stiff particles are immersed in a cementitious matrix. Alternatively, we can associate the intact and the degrading portions of a material system with the two families of degrees of freedom $\boldsymbol{r}_1$ and $\boldsymbol{r}_2$. In the case of cementitious particle composites, $\boldsymbol{K}_{12}, \boldsymbol{K}_{21}$ may be identified with the interface contact between the two solution domains where degradation often initiates, and where the two solution domains decouple progressively with increasing degradation.

(c) *Multiscale Partitions:* this is the field of *'upscaling'* from the micro-scale to the meso-scale, and from the meso-scale to the macro-scale. In the following, we explore the opportunities of *'Multiresolution Homogenization'* and discontinuous multi-wavelet transforms to extract the coarse grained solution at the macroscale from the fine grained solutions of the meso- and microscales. The field of computational homogenization is an exciting new area, Brewster and Beylkin [1995], Gilbert [1998], Beylkin and Coult [1998],(see also Steinberg and McCoy [1996], as well as Doborantu and Enquist [1998]), which has not been fully explored in the field of composite mechanics. An intriguing aspect of this methodology is the length scale, or in other terms, the footprint of the heterogeneity, i.e. the microstructural signature in the form of long range interaction. This length scale introduces a *'size-effect'* which transports localized defects from the micro-scale of observation to the macro-scale of homogenized continua which differs, however, from the fracture mechanics size argument of Bažant and Planas [1997].

Independently of the specific application at hand, let us examine the basic concept behind partitioning. The Schur complement of the partitioned system in Equation 1 generates the coarse grained solution $\boldsymbol{r}_1$ in the form of the 'REDUCTION' step:

$$[\boldsymbol{K}_{11} - \boldsymbol{K}_{12}\boldsymbol{K}_{22}^{-1}\boldsymbol{K}_{21}]\boldsymbol{r}_1 = \boldsymbol{f}_1 - \boldsymbol{K}_{12}\boldsymbol{K}_{22}^{-1}\boldsymbol{f}_2 \tag{2}$$

The fine scale response may be recovered from the 'RECONSTRUCTION' step which involves backward substitution in the form of,

$$\boldsymbol{r}_2 = \boldsymbol{K}_{22}^{-1}\boldsymbol{f}_2 - \boldsymbol{K}_{22}^{-1}\boldsymbol{K}_{21}\boldsymbol{r}_1 \tag{3}$$

The footprint of the condensed or rather the 'homogenized' stiffness depends on the effective spread of the triple product $\boldsymbol{K}_{12}\boldsymbol{K}_{22}^{-1}\boldsymbol{K}_{21}$ which defines the long range interaction of the solution domain in the spirit of the flexibility matrix as opposed to the stiffness matrix which normally exhibits only short range interaction because of the narrow band width. Aside from the computational aspects of linear algebra and direct equation solvers using L-U triangular factors instead of inverting the matrix partition $\boldsymbol{K}_{22}$ in the Schur

complement, the most important aspect of the reduction process is that it maintains ellipticity if the unreduced system is elliptic. In other terms, we are especially interested in partitions which remain stable at the coarse scale, but which might turn unstable at the fine scale at a given stage of the damage process. Thus one of the main issues revolves around the determinant partitioning theorem of Schur:

$$det(\boldsymbol{K}_o) = \det(\boldsymbol{K}_{22})\det(\boldsymbol{K}_{11} - \boldsymbol{K}_{12}\boldsymbol{K}_{22}^{-1}\boldsymbol{K}_{21}) \tag{4}$$

This important result states that the solution domain turns singular, i.e. $\det(\boldsymbol{K}_o) = 0$, if the Schur complement turns singular, i.e. $\det(\boldsymbol{K}_{11} - \boldsymbol{K}_{12}\boldsymbol{K}_{22}^{-1}\boldsymbol{K}_{21}) = 0$ when $\boldsymbol{K}_{11}$ degrades due to progressive damage, assuming $\det(\boldsymbol{K}_{22}) = c > 0$. Thereby, the determinant product of the two subdomains provides an upper bound of the coupled system, i.e.,

$$det(\boldsymbol{K}_o) \leq \det(\boldsymbol{K}_{11})\det(\boldsymbol{K}_{22}) \tag{5}$$

This upper bound estimate infers that the coupling effects have degraded to zero interaction, otherwise the positive triple product $\boldsymbol{K}_{12}\boldsymbol{K}_{22}^{-1}\boldsymbol{K}_{21}$ leads to an additional reduction of the deteriorating stiffness $\boldsymbol{K}_{11}$. This simple but intriguing result states that it is not only the deterioration of the subdomain, $\det(\boldsymbol{K}_{11}) \rightarrow 0$, which is responsible for the loss of ellipticity of the entire solution domain, but that the coupling partitions $\boldsymbol{K}_{12} = \boldsymbol{K}_{21}^t \neq \boldsymbol{0}$ play a very critical role when the entire system turns singular.

2.2 Damage Analysis of 1-dim Bar Problem

For illustration we examine the effect of progressive damage of the three bar problem shown in Figure 1. Let us assume that the intermediate element is subject to progressive damage leading to full erosion and let us examine how the constitutive damage process affects the positiveness of the serial bar structure. Assuming uniform material properties and uniform mesh size, the positive stiffness properties of each element are associated with the fundamental stretching mode $u_2 - u_1$ of each axial bar element. For definite-
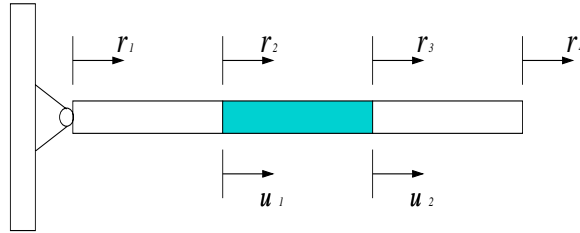

Figure 1: Deterioration due to element erosion in 1-D bar structure, $\frac{EA}{L}{=}1$

ness we assume that the elastic properties of the intermediate element are deteriorating progressively according to the traditional format of scalar damage,

$$\sigma = E_s\epsilon \quad \text{where} \quad E_s = [1 - D_E]E_o \quad \text{with} \quad D_E = 1 - \frac{E_s}{E_o} \tag{6}$$

Here E_o denotes the initial intact elastic modulus of elasticity, and D_E indicates the level of damage as a measure of the secant to the initial stiffness ratio. Considering different values of damage, $0 \leq D_E \leq 1$, Figure 2 illustrates the effect of material deterioration in the intermediate element on the spectral properties of the structure. In the present case of scalar damage, the element secant stiffness deteriorates proportionally to the material damage, i.e.

$$\boldsymbol{k}_s = \frac{[1 - D_E]E_o A}{L} \begin{bmatrix} 1 & -1 \\ -1 & 1 \end{bmatrix} \tag{7}$$

where $\frac{E_o A}{L} = 1$. Though the non-zero element eigenvalue decreases proportionally with progressive material damage, $\lambda_k = \frac{[1 - D_E]E_o A}{L}$, we observe in Figure 2(a) that deterioration at the structural level leads to non-proportional deterioration of all three eigenvalues. Normalization or rather pre-conditioning with the intact flexibility matrix $\boldsymbol{K}_o^{-1}$ separates the damage according to the rank-one update argument above, and leads to the spectral properties shown in Figure 2(b). We recognize, that pre-conditioning isolates the damage into a single eigenvalue associated with stretching the intermediate bar element the stiffness of which decreases proportionally with the level of material damage. The serial arrangement of the three bar elements leads to structural degradation according to the weakest link concept, such that the damage at the material level coincides with that of the weakest element and that of the entire structure, i.e. $D_E = D_k = D_K$.

Figure 3 illustrates the effect of material damage on the different partitions and on the corresponding contributions to the determinant according to the Schur theorem. It depicts the importance of separating the damage partition $\boldsymbol{K}_{11}$ from the intact stiffness $\boldsymbol{K}_{22}$, and the concomitant effect of the coupling partitions $\boldsymbol{K}_{12}$ and $\boldsymbol{K}_{21}$ which are responsible for singularizing the overall stiffness property. For further details see Willam and Rhee [2000].

3.0 Haar Wavelet Analysis

Wavelets are a means of representing a function in a hierarchical manner by a collection of coefficients and basis functions that can be used to recreate the original function. For example, the Haar basis [1910] is generated from a so-called *'mother function'* which results in averaging and differencing the original stiffness properties. This strategy may be used to create more general wavelet families, such as Meyer, Battle-Lemarie and Daubechies wavelets, (see e.g. Daubechies [1992]).

Wavelets have many useful properties which include:

(a) they are inexpensive to compute : the conversion to/from a wavelet representation can usually be performed in linear time,

(b) they generate multiresolution approximations : it is very easy to generate a lower-resolution approximation of a function using wavelets, by limiting the synthesis (reconstruction) process to a small number of levels. The approximation contains the broad characteristics of the original function,
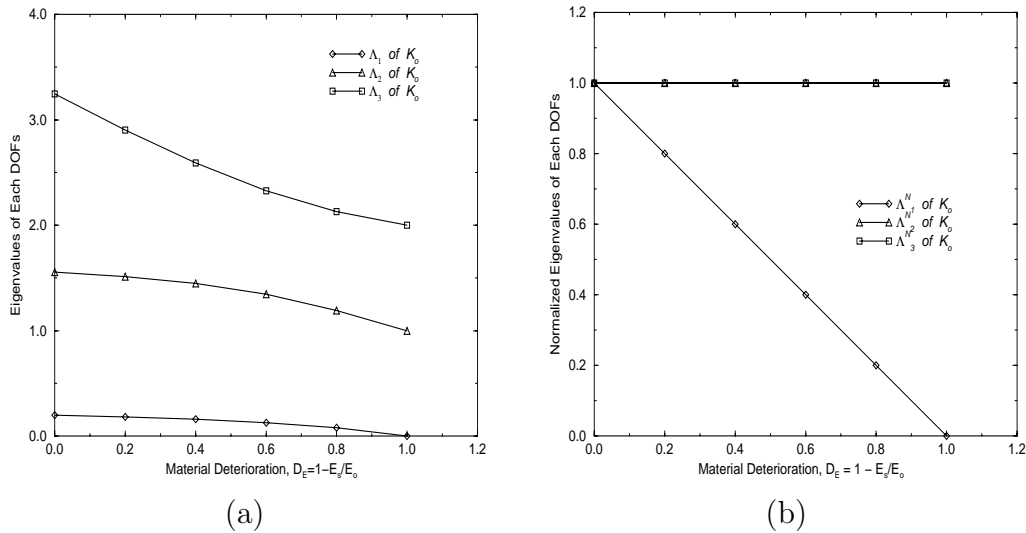
Figure 2: Three Bar Problem: Variation of (a) Eigenvalues, (b) Normalized Eigenvalues of Structural Assembly

(c) they introduce compact representation : the coefficients of a wavelet transfomation will often contain many small values or zeros. There are many compression schemes which can take advantage of this property to result in a reduction of memory needed to store the function. If an exact reconstruction of the original function is not required, small coefficient can be truncated to increase compression at the expense of accuracy of the reconstruction, and last not least,

(d) they are localized : unlike Fourier analysis, wavelets are able to handle localized functions with discontinuties, bounded domains, and non-periodic functions without any additional complexity. Localized wavelets are often used for the time-frequency description of signals when the localized time domain response needs to be reconstructed from individual frequency components.

The Haar wavelet [1910] is the earliest known example of a wavelet basis, and perhaps one of the simplest orthogonal basis. Hierarchical decomposition via filter banks transforms a signal in terms of the new basis. Thereby, the dilation equation

$$\phi(t) = \sqrt{2} \sum_k h_0(k) \phi(2t - k) \tag{8}$$

and the wavelet equation

$$\psi(t) = \sqrt{2} \sum_k h_1(k) \phi(2t - k) \tag{9}$$

are the main repositories where $\phi(t)$ is called the 'scaling function', and $\psi(t)$ is called the 'wavelet function'. The dilation equation and wavelet equation must hold for all t. Replacing t by $2^{j-1} t$ gives
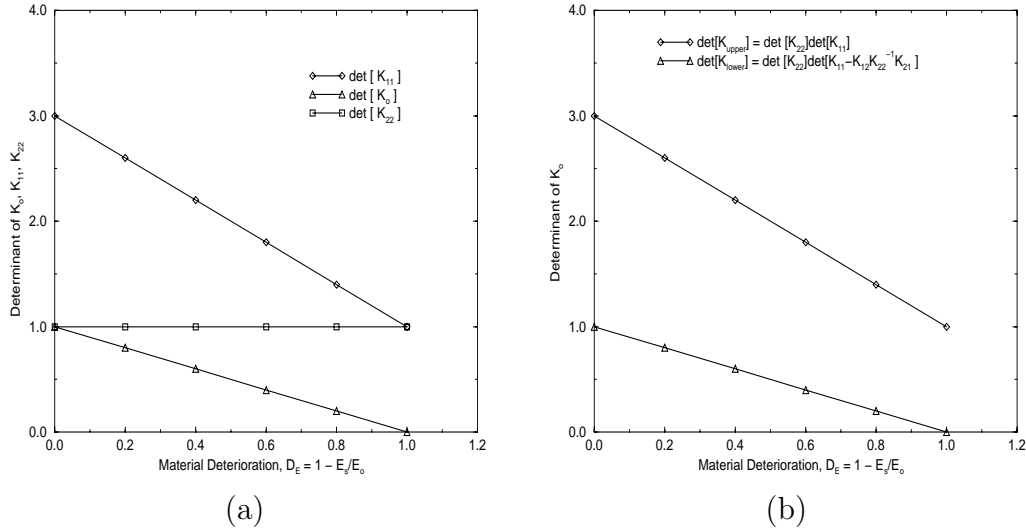
Figure 3: Three Bar Problem: Variation of (a) Determinant of the Assembly $\boldsymbol{K}_o$, and Partitions $\boldsymbol{K}_{11}$ and $\boldsymbol{K}_{22}$, (b) Upper Bound Property of Entire Assembly $\boldsymbol{K}_o$

$$\phi(2^{j-1}t) = \sqrt{2}\sum_k h_0(k)\phi(2^j t - k) \tag{10}$$

$$\psi(2^{j-1}t) = \sqrt{2}\sum_k h_1(k)\phi(2^j t - k) \tag{11}$$

In what follows we illustrate the wavelet basis construction from the dilation equations using the Haar filter bank. The low pass Haar filter $\boldsymbol{P}_n$ is defined by $h_0(0) = h_0(1) = 1/\sqrt{2}$ while all other coefficients are zero. Substituting the Haar low pass filter into Equation 8, we get

$$\phi(t) = \phi(2t) + \phi(2t - 1) \tag{12}$$

The solution to this recurrence is the Haar scaling function.

$$\phi(t) = \begin{cases} 1 & \text{if} \qquad t \in [0, 1); \\ 0 & \text{otherwise.} \end{cases} \tag{13}$$

The scaling function $\phi(t)$, $\phi(2t)$, and $\phi(2t - 1)$ is shown in Figure 4.
The high pass Haar filter $\boldsymbol{Q}_n$ is defined by $h_1(0) = 1/\sqrt{2}$ and $h_1(1) = -1/\sqrt{2}$. Substituting into Equation 9 yields

$$\psi(t) = \phi(2t) - \phi(2t - 1) \tag{14}$$
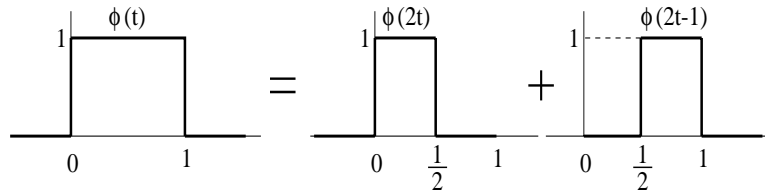
It follows that the Haar wavelet function is

Figure 4: The Haar scaling function $\phi(t)$, $\phi(2t)$, and $\phi(2t-1)$

$$\psi(t) = \begin{cases} 1 & \text{if} & t \in [0, \frac{1}{2}); \\ -1 & \text{if} & t \in [\frac{1}{2}, 1); \\ 0 & \text{otherwise.} \end{cases} \tag{15}$$
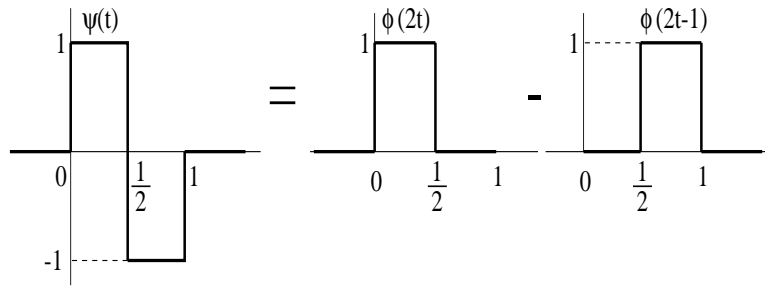
The wavelet function $\psi(t)$ is shown in Figure 5.

Figure 5: The Haar wavelet function $\psi(t)$

The scaling function $\phi(t)$ is the continuous analog of the discrete low pass filter $\boldsymbol{P}_n$. Applying $\phi(t)$ to $f(t)$

$$< \phi, f > = \int_{-\infty}^{\infty} \phi(t)f(t)dt = \int_0^1 f(t)dt \tag{16}$$

yields the average of f over the interval [0,1). The wavelet function $\psi(t)$ is the continuous analog of the discrete high pass filter $\boldsymbol{Q}_n$. Applying $\psi(t)$ to $f(t)$

$$< \psi, f > = \int_{-\infty}^{\infty} \psi(t)f(t)dt = \int_0^{\frac{1}{2}} f(t)dt - \int_{\frac{1}{2}}^1 f(t)dt \tag{17}$$

yields the difference of f over the interval [0,1). Consequently, the filter ϕ is an averaging operator, and the filter ψ is a differencing operator.

Now consider functions defined on the interval [0,1). Let V^j denote the set of functions that are constant on the 2^j subintervals $[l/2^j, (l+1)/2^j]$, $l = 0, 1, ..., 2^j - 1$. Any function in V^j can be represented exactly by a linear combination of the 2^j functions

$$\phi_{jk}(t) = \phi(2^j t - k), k = 0, \cdots, 2^j - 1 \qquad (18)$$

For the case j=3 the $2^j = 8$ resolution function is $\phi_{3k} = \phi(2^3 t - k), k = 0, ..., 7$.

Similarly, the wavelet functions are denoted by

$$\psi_{jk}(t) = \psi(2^j t - k), k = 0, ..., 2^j - 1 \qquad (19)$$

Figure 6 illustrates the sequence of scaling and wavelet transformations of three reductions by summing and differencing the unit step functions.
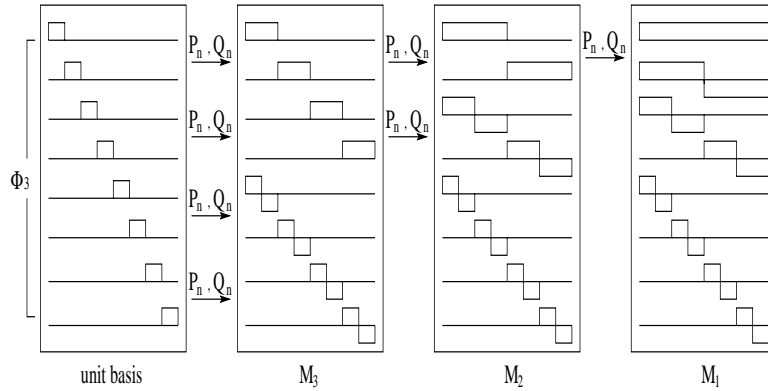

Figure 6: The Haar wavelet basis

As previously mentioned, Φ_j is the basis for V^j. Applying Equations 10 and 11 with $j = 3$ to the functions $\phi_{3k}(t) = \phi(2^3 t - k)$, $k = 0, \cdots, 7$ yields the functions $\phi_{2k}(t) = \phi(2^2 t - k)$, $k = 0, \cdots, 3$ and $\psi_{2k}(t) = \psi(2^2 t - k)$, $k = 0, \cdots, 3$.

In general, the Haar wavelet basis of V^j contains 2^j functions.

4.0 Multiresolution Homogenization

There are many important physical problems which incorporate several scales of observation. In heterogeneous media we typically encounter fine (microscopic) scale and coarse (macroscopic) scale features. Typically, *'homogenization'* methods require that the fine scale behavior is fairly well separated from the behavior on the coarse scales. Recently, a multiresolution analysis (MRA) has been proposed by Beylkin and Coult [1998] for homogenizing the transition between adjacent scales. This recursive procedure involves sequential steps of reduction as opposed to reconstruction, which may be repeated over many scales.

The basic step of the reduction involves computing a Schur complement which plays an important role in algebraic multigrid and domain decomposition methods. Thereby, the

form of equations is fully preserved so that one can use the reduction step in a recursive manner.

The main idea of the MRA scheme is illustrated best with the linear algebraic example,

$$\boldsymbol{K}\boldsymbol{r} = \boldsymbol{f}, \tag{20}$$

where $\boldsymbol{K}$ is a matrix of size $2^n \times 2^n$. We change basis by an orthogonal transformation with the discrete Haar transform by writing,

$$\boldsymbol{r}_s = \frac{1}{\sqrt{2}}(\boldsymbol{r}_{2k+1} + \boldsymbol{r}_{2k}) \text{ and } \boldsymbol{r}_d = \frac{1}{\sqrt{2}}(\boldsymbol{r}_{2k+1} - \boldsymbol{r}_{2k}) \tag{21}$$

for $k = 0, \cdots, 2^{n-1} - 1$. The elements of $\boldsymbol{r}_s$ are essentially averages of neighboring entries in $\boldsymbol{r}$ (they have an extra factor $\sqrt{2}$ when compared with true averages) and the elements of $\boldsymbol{r}_d$ are differences. We can write the discrete Haar transform as a matrix $\boldsymbol{M}_n$ of size $2^n \times 2^n$:

$$\boldsymbol{M}_n = \frac{1}{\sqrt{2}} \begin{bmatrix} 1 & 1 & 0 & 0 & & & \cdots \\ 0 & 0 & 1 & 1 & 0 & 0 & \cdots \\ & & & \ddots & & & \\ -1 & 1 & 0 & 0 & & & \cdots \\ 0 & 0 & -1 & 1 & 0 & 0 & \cdots \\ & & & \ddots & & & \end{bmatrix} \tag{22}$$

If we denote the top half of $\boldsymbol{M}_n$ by $\boldsymbol{P}_n$ and the bottom half by $\boldsymbol{Q}_n$, then

$$\boldsymbol{M}_n^t \boldsymbol{M}_n = \boldsymbol{M}_n \boldsymbol{M}_n^t = \boldsymbol{Q}_n^t \boldsymbol{Q}_n + \boldsymbol{P}_n^t \boldsymbol{P}_n = \boldsymbol{I} \text{ and } \boldsymbol{Q}_n \boldsymbol{Q}_n^t = \boldsymbol{I} = \boldsymbol{P}_n \boldsymbol{P}_n^t \tag{23}$$

Splitting the linear system in Equation 20 into two sets of equations in the two unknowns, $\boldsymbol{P}_n \boldsymbol{r} = \boldsymbol{r}_s$ and $\boldsymbol{Q}_n \boldsymbol{r} = \boldsymbol{r}_d$, and applying $\boldsymbol{P}_n$ to both sides, we get after dropping subscripts,

$$\boldsymbol{P}\boldsymbol{K}\boldsymbol{r} = (\boldsymbol{P}\boldsymbol{K}\boldsymbol{P}^t)\boldsymbol{P}\boldsymbol{r} + (\boldsymbol{P}\boldsymbol{K}\boldsymbol{Q}^t)\boldsymbol{Q}\boldsymbol{r} = \boldsymbol{P}\boldsymbol{f} \tag{24}$$

Similarly, if we apply $\boldsymbol{Q}_n$, we get

$$\boldsymbol{Q}\boldsymbol{K}\boldsymbol{r} = (\boldsymbol{Q}\boldsymbol{K}\boldsymbol{P}^t)\boldsymbol{P}\boldsymbol{r} + (\boldsymbol{Q}\boldsymbol{K}\boldsymbol{Q}^t)\boldsymbol{Q}\boldsymbol{r} = \boldsymbol{Q}\boldsymbol{f} \tag{25}$$

Denoting the partitions as,

$$\begin{aligned} \boldsymbol{K}_{ss} &= \boldsymbol{P}\boldsymbol{K}\boldsymbol{P}^t, \ \boldsymbol{K}_{sd} = \boldsymbol{P}\boldsymbol{K}\boldsymbol{Q}^t, \\ \boldsymbol{K}_{ds} &= \boldsymbol{Q}\boldsymbol{K}\boldsymbol{P}^t, \ \boldsymbol{K}_{dd} = \boldsymbol{Q}\boldsymbol{K}\boldsymbol{Q}^t, \\ \boldsymbol{f}_s &= \boldsymbol{P}\boldsymbol{f}, \text{ and } \boldsymbol{f}_d = \boldsymbol{Q}\boldsymbol{f} \end{aligned} \tag{26}$$

then, the transformed system reduces to

$$
\begin{bmatrix} \boldsymbol{K}_{ss} & \boldsymbol{K}_{sd} \\ \boldsymbol{K}_{ds} & \boldsymbol{K}_{dd} \end{bmatrix} \begin{bmatrix} \boldsymbol{r}_s \\ \boldsymbol{r}_d \end{bmatrix} = \begin{bmatrix} \boldsymbol{f}_s \\ \boldsymbol{f}_d \end{bmatrix} \tag{27}
$$

Assuming that $\boldsymbol{K}_{dd}$ is invertible we can solve for the fine scale variables $\boldsymbol{r}_d$ in terms of the coarse scale variables $\boldsymbol{r}_s$:

$$
\boldsymbol{r}_d = \boldsymbol{K}_{dd}^{-1} \boldsymbol{f}_d - \boldsymbol{K}_{dd}^{-1} \boldsymbol{K}_{ds} \boldsymbol{r}_s \tag{28}
$$

The reduced equation for the coarse scale dof $\boldsymbol{r}_s$ involves the Schur complement,

$$
[\boldsymbol{K}_{ss} - \boldsymbol{K}_{sd} \boldsymbol{K}_{dd}^{-1} \boldsymbol{K}_{ds}] \boldsymbol{r}_s = \boldsymbol{f}_s - \boldsymbol{K}_{sd} \boldsymbol{K}_{dd}^{-1} \boldsymbol{f}_d \tag{29}
$$

which determines the average values of $\boldsymbol{r}$. In other terms, we have an exact *'effective'* equation for the average of $\boldsymbol{r}_s$ which contains the contribution from the fine-scale behavior $\boldsymbol{r}_d$. Note that this reduced equation has half as many unknowns as the original system.

We should point out that under the reduction step the form of the original equation is fully preserved. Let $\boldsymbol{K}_j = \boldsymbol{K}$, $\boldsymbol{f}_j = \boldsymbol{f}$, $\boldsymbol{K}_{j-1} = \boldsymbol{K}_{ss} - \boldsymbol{K}_{sd} \boldsymbol{K}_{dd}^{-1} \boldsymbol{K}_{ds}$, and $\boldsymbol{f}_{j-1} = \boldsymbol{f}_s - \boldsymbol{K}_{sd} \boldsymbol{K}_{dd}^{-1} \boldsymbol{f}_d$. Then the algebraic system which governs the coarse scale $\boldsymbol{r}_s$ has the form $\boldsymbol{K}_{n-1} \boldsymbol{r}_s = \boldsymbol{f}_{n-1}$, where $\boldsymbol{r}_s = \boldsymbol{P}_{n-1} \boldsymbol{r}_j$ are our primary unknowns. This procedure can be repeated up to n times using the recursion formulas

$$
\begin{aligned}
\boldsymbol{K}_{j-1} &= \boldsymbol{K}_{ss} - \boldsymbol{K}_{sd} \boldsymbol{K}_{dd}^{-1} \boldsymbol{K}_{ds} \\
\boldsymbol{f}_{j-1} &= \boldsymbol{P}_{n-j} \boldsymbol{f}_j - \boldsymbol{K}_{sd} \boldsymbol{K}_{dd}^{-1} \boldsymbol{Q}_{n-j} \boldsymbol{f}_j
\end{aligned} \tag{30}
$$

where

$$
\begin{aligned}
\boldsymbol{K}_{ss} &= \boldsymbol{P}_{n-j} \boldsymbol{K}_j \boldsymbol{P}_{n-j}^t, \quad \boldsymbol{K}_{sd} = \boldsymbol{P}_{n-j} \boldsymbol{K}_j \boldsymbol{Q}_{n-j}^t \\
\boldsymbol{K}_{ds} &= \boldsymbol{Q}_{n-j} \boldsymbol{K}_j \boldsymbol{P}_{n-j}^t, \quad \boldsymbol{K}_{dd} = \boldsymbol{Q}_{n-j} \boldsymbol{K}_j \boldsymbol{Q}_{n-j}^t
\end{aligned} \tag{31}
$$

This recursion process involves only the matrices $\boldsymbol{K}_j$ and the vector $\boldsymbol{f}_j$. In other words, we do not have to solve for $\boldsymbol{r}$ at any step in the reduction procedure. If we apply this reduction process n times, we obtain a '$scalar$' SDOF equation which can be readily solved for the reduced load. This scalar equation furnishes the '$average$' response of the original $\boldsymbol{r}$- solution vector (up to the normalization $2^{\frac{n}{2}}$), i.e., the 'coarse' behavior. If we are only interested in this coarse behavior, then the reduction process gives us a way of determining exactly the average response without having to solve the original system $\boldsymbol{K} \boldsymbol{r} = \boldsymbol{f}$ for the unknown $\boldsymbol{r}$ and then computing its average. Of course, this multi-resolution technique is not faster than the best solvers of linear systems of algebraic equations. However, this example illustrates the technique which furnishes not only a single value for the homogenized stiffness property, but also the average solution of the coarse-scale behavior.
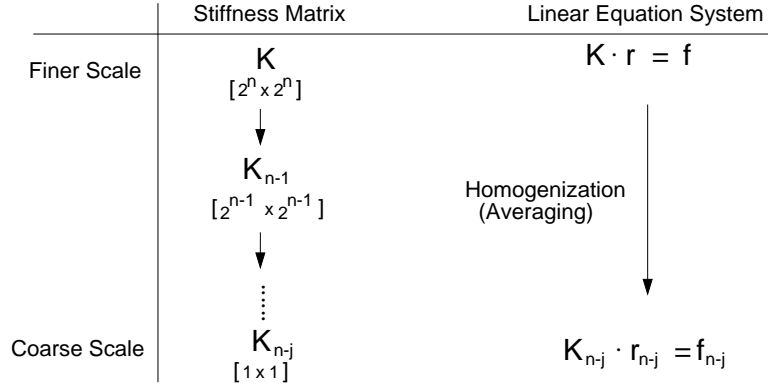
	Stiffness Matrix	Linear Equation System
Finer Scale	K $[2^n \times 2^n]$	$K \cdot r = f$
	$\downarrow$	
	K_{n-1} $[2^{n-1} \times 2^{n-1}]$	Homogenization (Averaging)
	$\downarrow$	$\downarrow$
	$\vdots$	
Coarse Scale	K_{n-j} $[1 \times 1]$	$K_{n-j} \cdot r_{n-j} = f_{n-j}$

Figure 7: MRA Reduction Procedure

5.0 Bounding Properties

An important observation is that the reduction process constrains the dof, thus it provides an upper bound of the estimate of ellipticity. In other terms, the eigenvalues of the reduced system are bounded by the lowest and highest eigenvalue of the unreduced system. This result is well-known in the field of domain-decomposition methods, where the Schur complement plays a prominent role, but it is not well-established in the field of mechanics and materials.

5.1 Rayleigh-Ritz Bounds

Bounds of the reduction process may be readily developed from the Rayleigh-Ritz argument which states that the quadratic forms of the stiffness matrix is bounded below by the minimum eigenvalue and bounded above by the maximum eigenvalue of $\boldsymbol{K}_o$,

$$\lambda_{min} \leq \boldsymbol{r}^t \boldsymbol{K}_o \boldsymbol{r} \leq \lambda_{max} \quad \forall \boldsymbol{r} \neq \boldsymbol{0} \tag{32}$$

In the terminology of mechanics and materials, these eigenvalues represent the strain energy stored in the material system. Because of the orthogonality of the wavelet transformation the spectral properties of the original system are preserved, but those of the reduced system $\boldsymbol{R}_j = \boldsymbol{K}_{ss} - \boldsymbol{K}_{sd}\boldsymbol{K}_{dd}^{-1}\boldsymbol{K}_{ds}$ are bounded above and below because of the static condensation process, i.e.

$$\lambda_{min} \leq \boldsymbol{r}_s^t \boldsymbol{R}_j \, \boldsymbol{r}_s \leq \lambda_{max} \quad \forall \boldsymbol{r}_s \subset \boldsymbol{r} \neq \boldsymbol{0} \tag{33}$$

5.2 Preservation of Ellipticity

The issue is how large is the reduction effect on the lowest eigenvalue. Following the arguments of Beylkin and Coult [1998], ellipticity is preserved if the original stiffness is positive definite. They also showed that in the process of reduction small eigenvalues are well preserved. We will show below that the lowest eigenvalue of the unreduced system is increasing very little during each reduction step which will be illustrated with one- and two-dimensional example problems in Section 6.

Let $\boldsymbol{K}_j$ be a self-adjoint, positive-definite operator on V_j, such that

$$m\|\boldsymbol{r}\|^2 \leq \boldsymbol{r}^t \boldsymbol{K}_j \boldsymbol{r} \leq M\|\boldsymbol{r}\|^2 \quad \forall \boldsymbol{r} \in V_j \tag{34}$$

where $0 < m \leq M$. Then the spectral properties of the reduced system maintain the upper and lower bounds of the unreduced system, i.e.

$$m\|\boldsymbol{r}\|^2 \leq \boldsymbol{r}^t \boldsymbol{R}_j \boldsymbol{r} \leq M\|\boldsymbol{r}\|^2 \quad \forall \boldsymbol{r} \in V_{j+1} \tag{35}$$

Using the reduction transformations we can write

$$\begin{aligned} \boldsymbol{K}_{ss} &= \boldsymbol{P}_{j+1} \boldsymbol{K}_j \boldsymbol{P}_{j+1}^t, \\ \boldsymbol{K}_{sd} &= \boldsymbol{P}_{j+1} \boldsymbol{K}_j \boldsymbol{Q}_{j+1}^t = \boldsymbol{K}_{ds}^t, \\ \boldsymbol{K}_{dd} &= \boldsymbol{Q}_{j+1} \boldsymbol{K}_j \boldsymbol{Q}_{j+1}^t, \end{aligned} \tag{36}$$

Therefore, we have

$$\boldsymbol{R}_j = \boldsymbol{K}_{ss} - \boldsymbol{K}_{sd} \boldsymbol{K}_{dd}^{-1} \boldsymbol{K}_{ds} = \boldsymbol{R}_j^t \tag{37}$$

Since $\boldsymbol{K}_j$ is positive definite, so is $\begin{bmatrix} \boldsymbol{K}_{ss} & \boldsymbol{K}_{sd} \\ \boldsymbol{K}_{ds} & \boldsymbol{K}_{dd} \end{bmatrix}$, it follows that $\boldsymbol{K}_{dd}$ is positive definite and $\boldsymbol{K}_{dd}^{-1}$ exists. Introducing the operator

$$\boldsymbol{Z} = \begin{bmatrix} \boldsymbol{I} & \boldsymbol{0} \\ -\boldsymbol{K}_{dd}^{-1} \boldsymbol{K}_{ds} & \boldsymbol{I} \end{bmatrix} \tag{38}$$

Then the $\boldsymbol{Z}$-transformation leads to block diagonal form,

$$\boldsymbol{Z}^t \begin{bmatrix} \boldsymbol{K}_{ss} & \boldsymbol{K}_{sd} \\ \boldsymbol{K}_{sd}^t & \boldsymbol{K}_{dd} \end{bmatrix} \boldsymbol{Z} = \begin{bmatrix} \boldsymbol{R}_j & \boldsymbol{0} \\ \boldsymbol{0} & \boldsymbol{K}_{dd} \end{bmatrix} \tag{39}$$

Consequently the quadratic form,

$$\boldsymbol{r}^t \boldsymbol{R}_j \boldsymbol{r} = \begin{bmatrix} \boldsymbol{r} \\ \boldsymbol{0} \end{bmatrix}^t \begin{bmatrix} \boldsymbol{Z}^t \begin{bmatrix} \boldsymbol{K}_{ss} & \boldsymbol{K}_{sd} \\ \boldsymbol{K}_{sd}^t & \boldsymbol{K}_{dd} \end{bmatrix} \boldsymbol{Z} \end{bmatrix} \begin{bmatrix} \boldsymbol{r} \\ \boldsymbol{0} \end{bmatrix}, \tag{40}$$

yields the lower bound of the reduced system as

$$\boldsymbol{r}^t \boldsymbol{R}_j \boldsymbol{r} \geq m(\|\boldsymbol{K}_{dd}^{-1} \boldsymbol{K}_{ds} \boldsymbol{r}\|^2 + \|\boldsymbol{r}\|^2) \geq m\|\boldsymbol{r}\|^2 \tag{41}$$

To estimate the upper bound, we use $\boldsymbol{R}_j + \boldsymbol{K}_{sd}\boldsymbol{K}_{dd}^{-1}\boldsymbol{K}_{ds} = \boldsymbol{K}_{ss}$ and positive definiteness of $\boldsymbol{K}_{dd}^{-1}$ to obtain the bound

$$(\boldsymbol{r}^t \boldsymbol{R}_j \boldsymbol{r}) \leq (\boldsymbol{r}^t \boldsymbol{K}_{ss} \boldsymbol{r}) \tag{42}$$

Since the partitioned matrix after wavelet transformation $\begin{bmatrix} \boldsymbol{K}_{ss} & \boldsymbol{K}_{sd} \\ \boldsymbol{K}_{sd}^t & \boldsymbol{K}_{dd} \end{bmatrix}$ satisfies the same spectral bounds as $\boldsymbol{K}_j$, we have the upper bound property given in terms of

$$(\boldsymbol{r}^t \boldsymbol{K}_{ss} \boldsymbol{r}) \leq M \|\boldsymbol{r}\|^2 \tag{43}$$

Since we made no assumptions other than orthogonality about the multiresolution analysis, the bounding properties do not depend on dimension or the choice of wavelet basis.

The ellipticity estimate of Equation 35 raises the important question under which conditions do the lower eigenvalues of $\boldsymbol{K}_j$ coincide with the eigenvalues of $\boldsymbol{R}_j$ and how close are the upper bounds. Clearly, the answer to this question depends on how well the fundamental modes of the unreduced system are captured by the reduced system.

6.0 Homogenization of Two-Phase Particle Composites

In what follows we consider the homogenization of a two-phase particle composite which is made up of elastic aggregate inclusions which are embedded in an elastic matrix. For illustration we compare homogenization via MRA in one- and two-dimensions in order to assess the validity of the homogenization parameter and its bounding property when compared to averaging the numerical FEM results.

6.1 One-dimensional Model Problem

To start with we consider a periodic arrangement of stiff particles and weak matrix constituents in the one-dimensional simulation model shown in Figure 8, for which analytical solutions are readily available from homogenization.

Assuming linear elastic behavior of the two materials with a contrast ratio of the stiffness properties $E_a/E_m = 3$ with $E_m = 10$, the spectral properties of the $ndof = 2^6 = 64$ simulation with 64 bar elements of size $h = 1$ range from $\lambda_{min} = 8.82701 \times 10^{-3}$ to $\lambda_{max} = 7.99647 \times 10^1$. After six cycles of reduction the homogenization parameter results in the *'average'* stiffness property $K_{ss}^{homog} = 1.06101 \times 10^{-2}$ at the coarse scale of a single degree of freedom problem, SDOF.

Further on we note that linear analysis of the initial 64 dof system results in the average axial displacement $\bar{r}_{64}^{FEM} = 2.1833$. In fact, recursive averaging of the fine grained solution does not affect the overall solution at all. In other terms, the homogenized solution of the coarse SDOF system $\bar{r}^{MRA} = 2.1833$ coincides with the results of the original fine grained solution using the scale factor $\sqrt{2}^6$. Moreover, the response of the one-dimensional serial

structure is in full agreement with the homogenized response of composite mechanics $r_{homog}^{Reuss} = 2.1833$, whereby the effective moduli of Reuss provide a lower bound which happens to reproduce the exact solution in the case of the serial bar structure.

Figure 9(a) illustrates the gradual increase of the minimum eigenvalues at each reduction step which maintain a very close upper bound of the lowest eigenvalue of the unreduced system. The figure illustrates that the lowest eigenvalue hardly increases except in the final two steps of reduction. Figure 9(b) shows the effect of degradation of the aggregate constituents on the lowest eigenvalue, both for the unreduced as well as for the homogenized bar structure after six steps of reduction. We observe the upper bound property of the homogenization parameter when compared with the lowest eigenvalue of the unreduced system, whereby the singularity of the fully damaged serial structure is reproduced by the homogenization parameter when $D_E \to 1$.

Figure 10(a) illustrates the effect of material damage on the stiffness properties of the unreduced system and the two partitions shown in Figure 12(b) of the homogenized system after six reductions. The figure illustrates that all determinants diminish as $D_E \to 0$ since the damaging dof were not separated from the intact dof. Figure 10(b) shows the effect of aggregate degradation on the determinant product of the two partitions for the homogenized bar structure which provides an upper bound property of the coupled system using the Schur complement. Thereby the singularity of the fully damaged serial structure when $D_E \to 1$ is reproduced by both determinant measures including its upper bound.

The sparse structure of the narrow band in the original (64×64) stiffness is illustrated in Figures 11(a) and (b), and in Figures 12(a) and (b) together with their Haar transformations after three and five reduction steps. The grey shadings indicate the sparse population of matrices at the reduction steps R^{64}, R^8, R^1, whereby the intensity is a measure of the absolute magnitude of the stiffness coefficient.

In short, MRA provides a homogenized stiffness property which reproduces exactly the average response for a given load scenario, whereby the resulting homogenization parameter maintains a close upper bound of the lowest eigenvalue of the unreduced bar structure.

6.2 Two-Dimensional Model Problem

In what follows we consider homogenization of the two-phase particle composite in 2-dimension as indicated in Figure 13(a) and (b).

Assuming isotropic linear elastic behavior of the two materials with a contrast ratio of the stiffness properties $E_a/E_m = 3$ and $\nu_a/\nu_m = 0.5$, the spectral properties of the $ndof = 2^{10} = 1024$ simulation range from $\lambda_{min} = 5.293 \times 10^{-2}$ to $\lambda_{max} = 2.125 \times 10^2$. Given the volume fraction of the aggregate particles, $V_a = 0.346917$, the Hashin-Shtrikman bounds of the effective stiffness properties are $15.2889 \geq E^{eff} \geq 14.2114$ and $0.133763 \leq \nu \leq 0.142968$. After MRA through 10 reduction cycles, the homogenization parameter results in the equivalent stiffness $K_{ss}^{homog} = 10.1275$ which leads to the average value of relative displacement $\bar{r}^{MRA} = 0.3165$ using the scale factor $\sqrt{2}^{10}$.
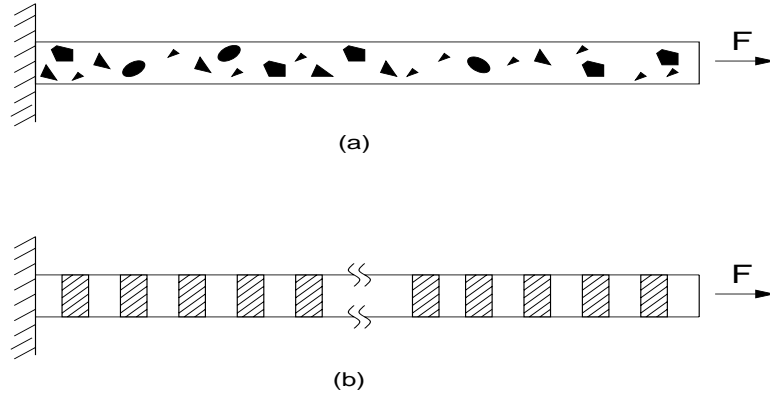
Figure 8: 1-dim. Axial Bar Problem Made of Periodic 2-Phase Material

The sparse population of the reduced stiffness matrices are shown in Figures 14, 15 and 16, after three, eight and nine cycles of reduction. Thereby the level of grey shading indicates the absolute magnitude of the stiffness coefficients in the coarse and fine partitions at different levels of observation.

Figure 17(a) finally illustrates the increase of the minimum eigenvalue at each reduction step which maintains a close upper bound of the lowest eigenvalue of the unreduced system. Figure 17(b) shows the effect of the material deterioration on the homogenization parameter of the fully reduced 2-dim. structure, (i) when the matrix, and (ii) when the aggregate properties are damaged progressively. In the limit the homogenization parameter fully reproduces the singularity of the composite structure when either the matrix or the aggregate constituents are fully damaged , i.e. $D_E \rightarrow 1$.

It is particularly noteworthy to compare the results of the scalar reduction at cycle 10 with the vectorial reduction at cycle 9 of the average displacements in the x-y directions comparing the stiffness populations in Figure 14 and Figure 15. This separation provides insight into the elastic response of the heterogeneous panel when subjected to uniform tension in the y-direction. This separation is necessary to reconstruct tensor-valued results of elasticity from the homogenized vector field of displacements. In other terms the reconstruction of average stresses and strains leads to additional questions how to extract consistent values of homogenized stresses and strains from the average of relative displacements.

7.0 Conclusion

In this paper, we presented a novel homogenization method to separate coarse from fine scale features based on a recursive Schur reductions combined with Haar wavelet transforms. Thereby, the finite element methodology was utilized to assess the homogenized stiffness which provides a close upper bound of the lowest eigenvalue.
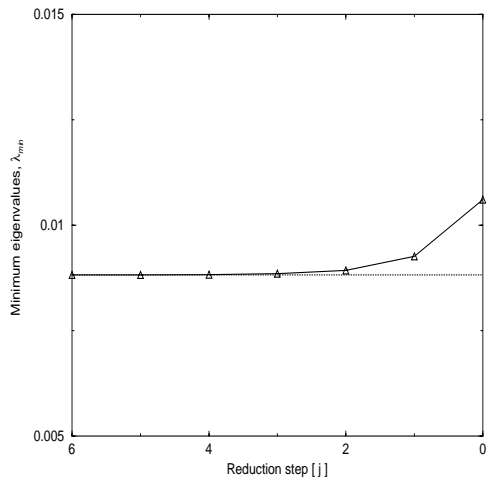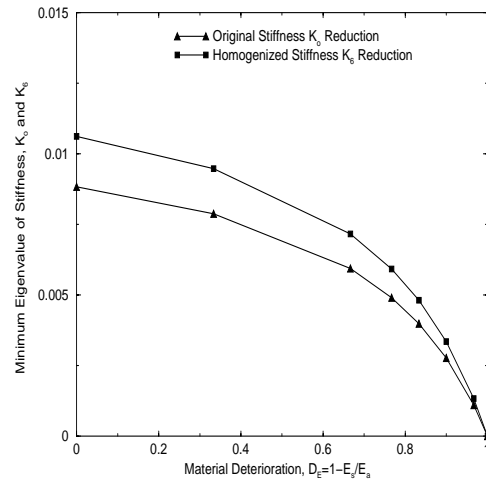
Figure 9: 1-dim. Axial Bar Problem: (a) Upper Bound Properties of Minimum Eigenvalues at Different Cycles of Reduction in 1-dim. (b) Variation of Minimum Eigenvalue of Stiffness, $\boldsymbol{K}_o$ and $\boldsymbol{K}_6$ due to Progressive Deterioration of Aggregate Stiffness.

Two example problems were used to illustrate the recursive methodology. Application to two-phase particle composites did exhibit a number of salient features. It demonstrated that the reduction procedure maintains ellipticity and provides a close upper bound of the fundamental mode a long as the unreduced problem is positive definite. On the other hand, progressive damage introduces zero stiffness properties in portions of the solution domain which does result in singular properties of the unreduced material system. It is remarkable that this singularity is fully reproduced by the homogenization parameter in spite of the upper bound properties of the reduced system.

Although our observations were based on fairly elementary concepts of static condensation and orthogonal wavelet transforms of the elastic stiffness properties of heterogeneous materials, they provide a first step towards homogenization and MRA analysis of path-dependent nonlinear material systems.

8.0 Acknowledgements

(a)   (b)
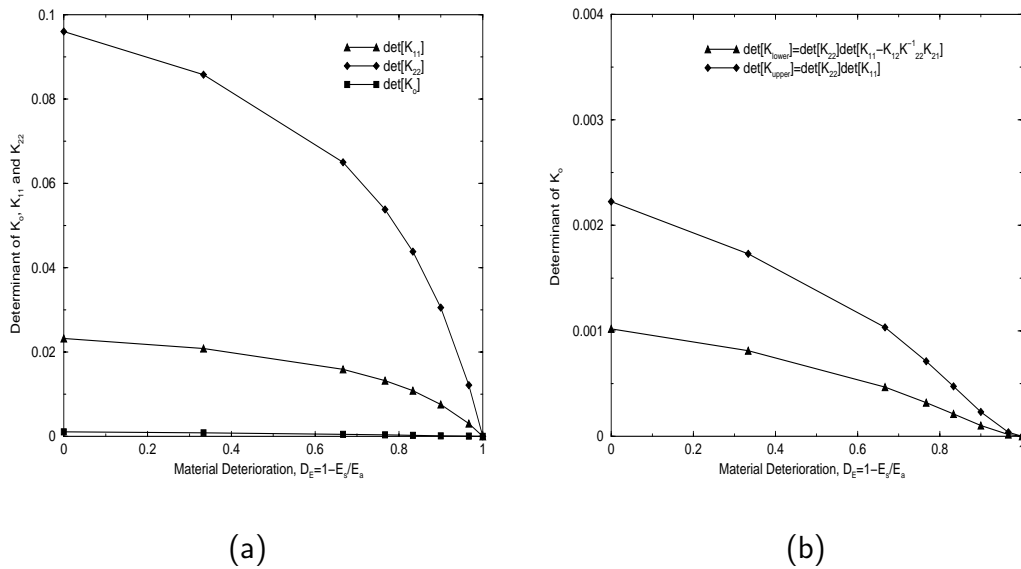
Figure 10: 1-dim. Axial Bar Problem: (a) Effect of Material Degradation on Determinant of Unreduced Bar Problem $\boldsymbol{K}_o$, and the Homogenized Partitions $\boldsymbol{K}_{11}$, $\boldsymbol{K}_{22}$ after six Reductions, (b) Upper Bound Property of Determinant Product after six Reductions.

References

[1] Bažant, Z. P. and Planas, J., Fracture and Size Effect in Concrete and other Quasibrittle Materials. *CRC Press*, Boca Raton, FL. (1997).

[2] Beylkin, G. and Coult, N. *'A Multiresolution Strategy for Reduction of Elliptic PDE's and Eigenvalues Problems'*, Applied and Computational Harmonic Analysis, 5 (1998) 847-897.

[3] Brewster, M. E. and Beylkin, G. *'A Multiresolution Strategy for Numerical Homogenization'*, Applied and Computational Harmonic Analysis, 2 (1995) 327-349.

[4] Daubechies, I. Ten Lectures on Wavelets, Society for Industrial and Applied Mathematics (*SIAM*), (1992).

[5] Dorobantu, M. and Engquist, B. *'Wavelet-Based Numerical Homogenization'*, SIAM Journal on Numerical Analysis, 35 (1998) 540–559.

[6] Gilbert, A. *'A Comparison of Multiresolution and Classical Homogenization Schemes'*, Applied and Computational Harmonic Analysis, 5 (1998) 1-35.

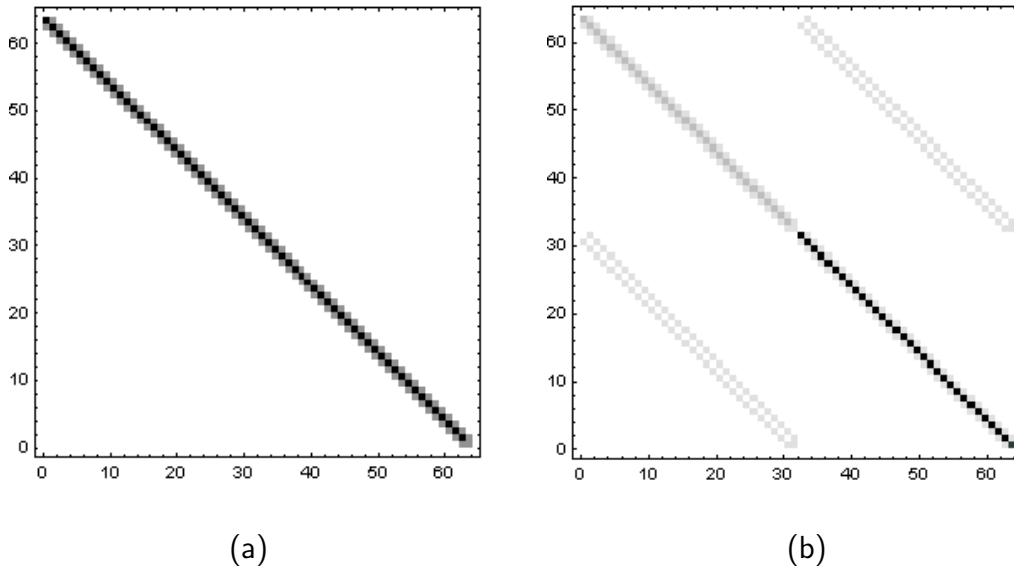[7] Haar, A. *'Zur Theorie der orthogonalen Funktionensysteme'*, Math. Annalen, 69 (1910) 331-371.

(a)	(b)

Figure 11: 1-dim. Axial Bar Problem, Density Plot of Stiffness Matrix: (a) $\boldsymbol{K}_6 \in \mathcal{R}^{64}$, (b) $\boldsymbol{M}_6 \boldsymbol{K}_6 \boldsymbol{M}_6^t \in \mathcal{R}^{64}$

[8] Hashin, Z. *'Analysis of Composite Materials'*, Journal of Applied Mechanics, ASME, 50 (1987) 481-505.

[9] Rizzi, E., Maier, G. and Willam, K. *'On Failure Indicators in Multi-Dissipative Materials'*, Intl. J. Solids Structures, 33:20-22 (1996) 3187-3214.

[10] Schur, I. *'Ein Beitrag zur additiven Zahlentheorie und zur Theorie der Kettenbrüche'*, S.B. Preuss. Akad. Wiss. Phys-Math. Kl., (1917) 302-321 (reprinted in I. Schur, Gesammelte Abhandlungen, 2, Springer Verlag 1973, 117-136).

[11] Sternberg, B.Z. and McCoy, J.J. *'A Class of One-dimensional Stiffness Microstructures Resulting in Identical Macroscale Response'*, Wave Motion, 23 (1996) 237-258.

[12] Willam, K. and Rhee, I. *'Deterioration Analysis of Materials and Finite Elements'*, Engineering Computations: Intl. J. Comp. Aided Engrg. & Software, 18/3-4 (2000) 690-718.
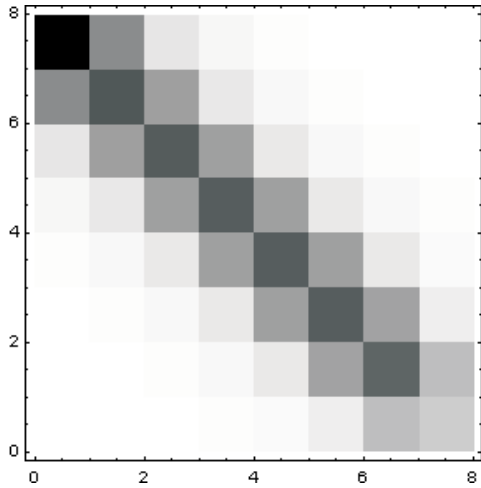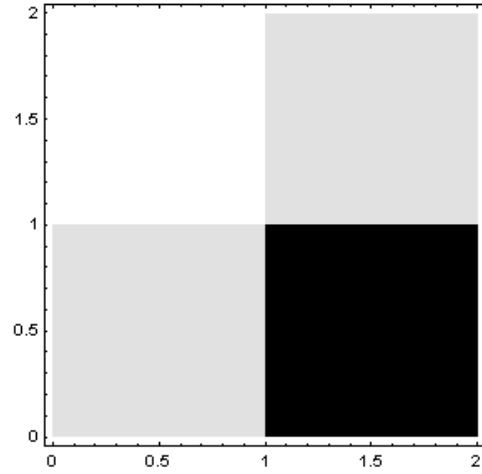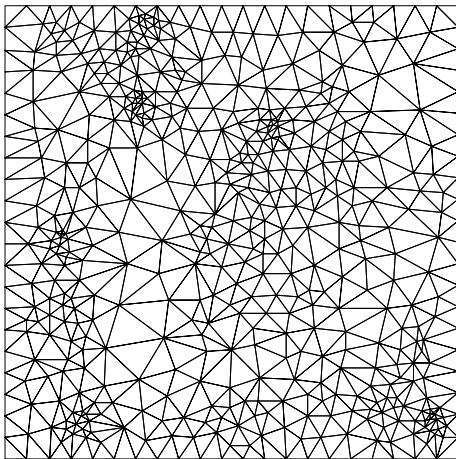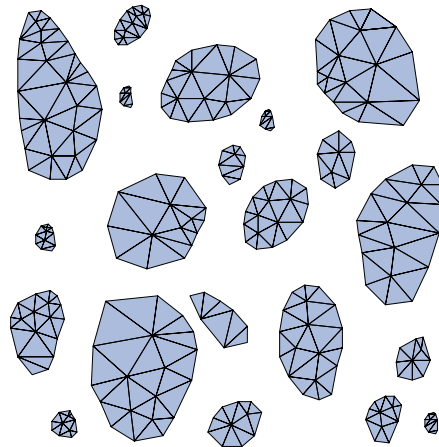
Figure 12: 1-dim. Axial Bar Problem, Density Plot of Stiffness Matrix: (a) $\boldsymbol{K}_3 \in \mathcal{R}^8$, (b) $\boldsymbol{M}_1 \boldsymbol{K}_1 \boldsymbol{M}_1^t \in \mathcal{R}^1$

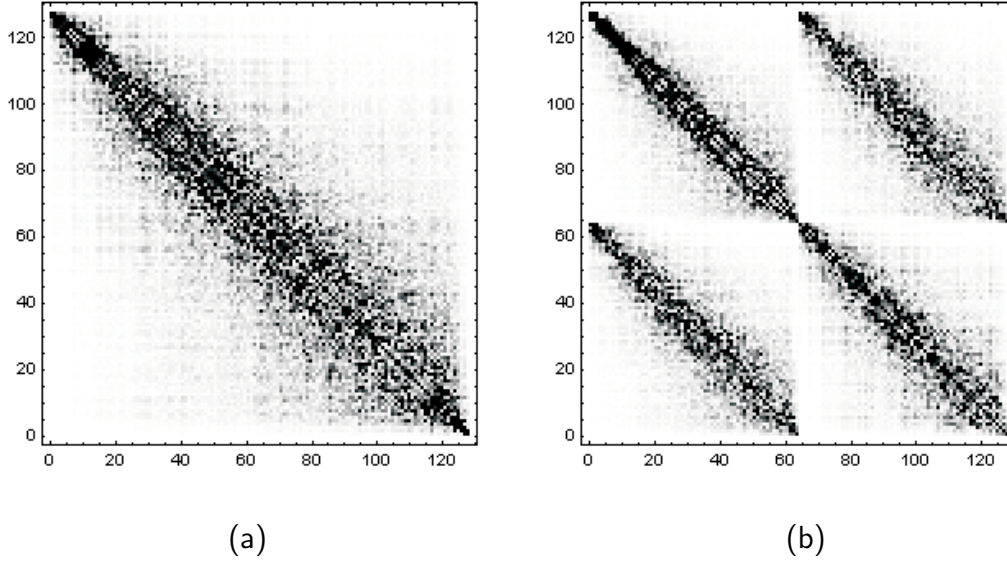Figure 13: 2-dim. Composite Structure: (a) Overall Mesh (b) Aggregates Mesh

Figure 14: 2-dim. Composite Structure, Density Plot of Stiffness Matrix: (a) $\boldsymbol{K}_7 \in \mathcal{R}^{128}$, (b) $\boldsymbol{M}_7\boldsymbol{K}_7\boldsymbol{M}_7^t \in \mathcal{R}^{128}$
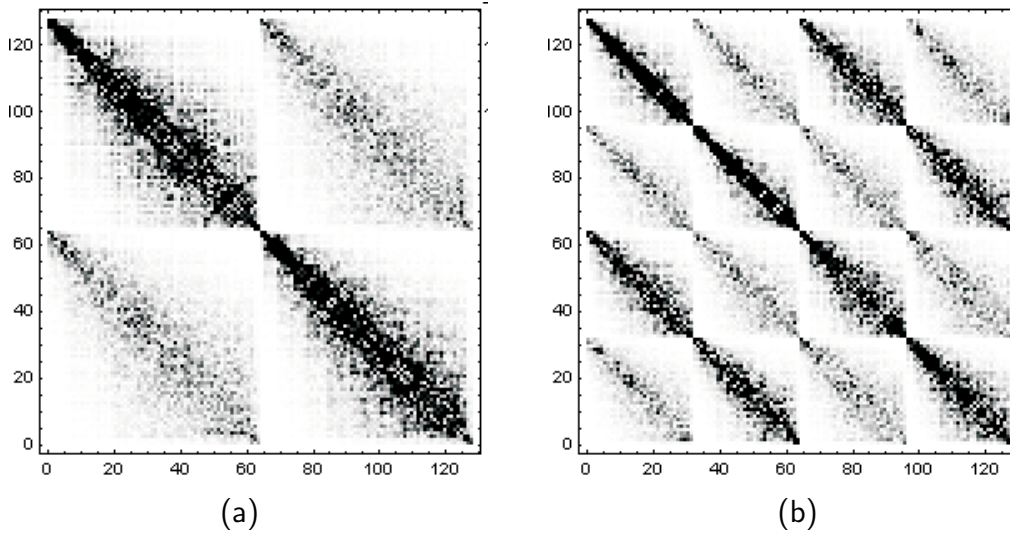

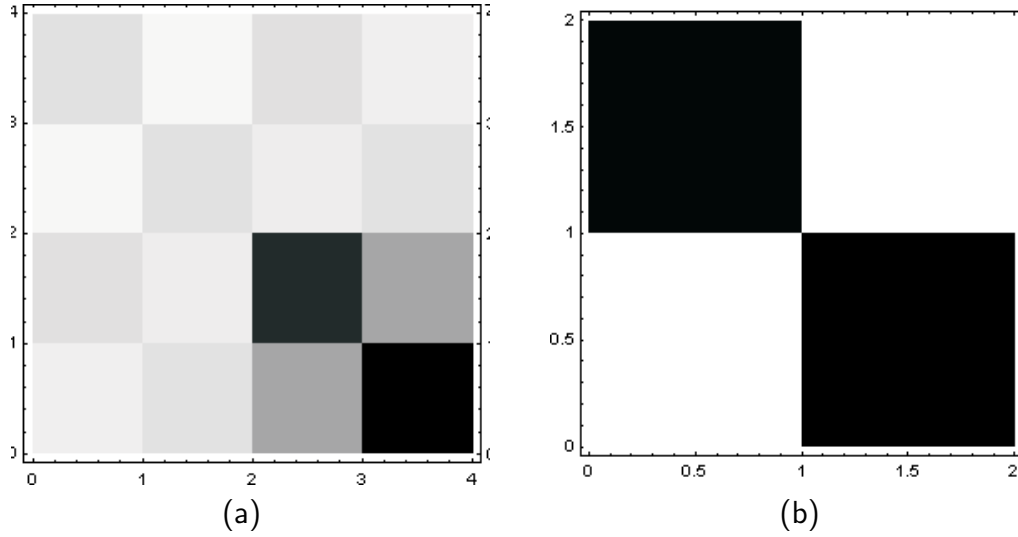Figure 15: 2-dim. Composite Structure, Density Plot of Separating x-, y-Stiffness Coefficients: (a) $\boldsymbol{K}_7 \in \mathcal{R}^{128}$, (b) $\boldsymbol{M}_7\boldsymbol{K}_7\boldsymbol{M}_7^t \in \mathcal{R}^{128}$

Figure 16: 2-dim. Composite Structure, Density Plot of Separating x-, y-Stiffness Coefficients: (a) $\boldsymbol{M}_2 \boldsymbol{K}_2 \boldsymbol{M}_2^t \in \mathcal{R}^4$, (b) $\boldsymbol{M}_1 \boldsymbol{K}_1 \boldsymbol{M}_1^t \in \mathcal{R}^2$
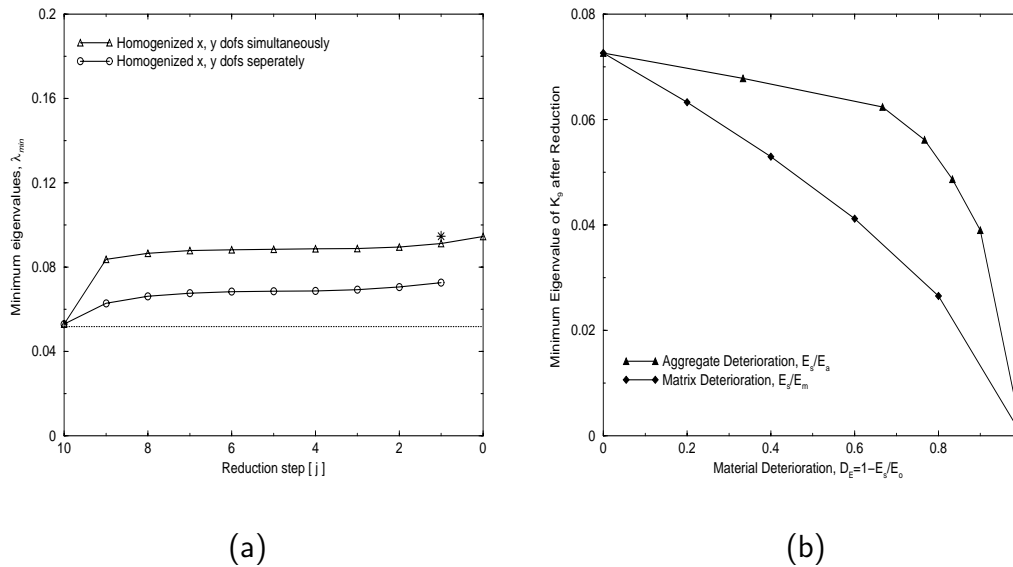

Figure 17: 2-dim. Composite Structure: (a) Upper Bound Properties of Minimum Eigenvalues at Different Cycles of Reduction b) Homogenized Stiffness Reduction due to Matrix/Aggregate Deterioration when $D_E \to 1$.